Plasmonics
DOI 10.1007/s11468-016-0337-8

Spoof Localized Surface Plasmons Excited by Plasmonic Waveguide Chip with Corrugated Disk Resonator

Danni Wang[1] · **Lin Chen**[1,2,3] · **Bo Fang**[1,2] · **Yiming Zhu**[1,3]

Received: 26 April 2016 / Accepted: 6 July 2016

Abstract We designed and fabricated a millimeter plasmonic chip consisted of coplanar waveguide (CPW) and plasmonic waveguide with one corrugated disk resonator (CDR). The spoof localized surface plasmon (LSP) resonance modes can be excited by the interaction between plasmonic waveguide and CDR. Fundamental and higher order sharp spoof LSP resonances (from dipole to dodecapole) were observed in the transmission coefficient spectrum. The Q-value as high as 268.3 (octupole) was experimentally obtained. Experimental results show good agreement with theoretical and simulated ones. All the results may have potential applications in microchip based sensing and filtering.

Keywords Corrugated disk resonator · Coplanar waveguide · Spoof localized surface plasmons · Multichannel

✉ Lin Chen
linchen@usst.edu.cn

Yiming Zhu
ymzhu@usst.edu.cn

[1] Shanghai Key Lab of Modern Optical System, Engineering Research Center of Optical Instrument and System, Ministry of Education, University of shanghai for Science and Technology, No.516 JunGong Road, Shanghai 200093, China

[2] College of Metrology and Measurement Engineering, China Jiliang University, Hangzhou 310018, People's Republic of China

[3] Cooperative Innovation Centre of Terahertz Science, University of Electronic Science Chengdu, Chengdu 611731, People's Republic of China

Introduction

Recently, high Q-value millimeter-wave sensors have attracted a great deal of attention, due to their applications on food safety, biomedical detection, and security instrument [1]. There are several designs to achieve such sensors with high Q-value feature, such as thin metamaterial plate [2, 3], prism-coupled system [4], and parallel plate waveguide [5–8]. However, sensors mentioned above have some disadvantages. For example, prism-coupled system and parallel plate waveguide cavities-based sensors could achieve high-Q value in the transmission spectrum, and the structures are very simple, but the prism or metal bulks hinder the integration of sensor. Plasmonic metamaterial sensors, such as metal holes array structure [9] and split ring resonators (SRRs) [10], can present Fabry Perot effect from front and back surfaces of the substrate, resulting in the transmission signal distortion [11]. Recently, planar millimeter-wave chips are proposed to accomplish low loss propagation and resonator for integration. Especially, Ma et al. [12] proposed the high efficient coupling from traditional coplanar waveguide (CPW) to plasmonic waveguide. Then, some plasmonic chips were designed by using this efficient coupling method, such as surface plasmon polaritons amplifier [13] and controlling rejection filter [14]. Such chips can be used in biosensing application, due to the fact that the evanescent field of spoof LSP mode is sensitive to the refractive index of the material and only a small amount of sample is required. To achieve multichannel biosensing application, several SRRs with different size were designed to accomplish multichannel resonances in the transmission coefficient spectrum [14]. But the mutual coupling

Published online: 16 July 2016

between two close SRRs may produce interference and have influence on the transmission results.

In this paper, multichannel resonances can be easily obtained in plasmonic chip comprised of plasmonic waveguide and corrugated disk resonator (CDR). Spoof LSP modes are excited in CDR and show multipolar resonances similar to those at terahertz frequencies [15]. A gradient plasmonic Vivaldi slot is used to efficiently match the momentum between CPW and plasmonic waveguide [12]. So, it is easier to extend the frequency range from millimeter to terahertz than coaxial line coupling [16]. In addition, these spoof LSP resonances are observed experimentally by using vector network analyzer. Since the proposed chip is compact and easy to be integrated, it may have applications in multichannel sensing and filters.

Design and Simulation

The designed millimeter chip is illustrated in Fig. 1. The plasmonic waveguide port 1 and 2 can be used as signal input and output port, respectively. The structure includes three parts: I. an energy transition section, II. mode conversion and momentum matching section, and III. plasmonic waveguide with CDR. Part I is CPW that supports the quasi transverse electromagnetic (QTEM) mode of guided waves [14]. The CPW impedance is determined by the parameters of the port. Here, we choose the width of waveguide port w (100 μm), the width of slot lines g (9.4 μm), and the permittivity ε of quartz substrate (3.75) to ensure impedance matching. Part II is the convertor that transits from QTEM mode to spoof surface plasmons mode. It should be pointed out that there is the strong momentum mismatch between CPW and plasmonic waveguide. Here, the gradient grooves with two symmetrically exponential slot lines (input and output) are introduced to achieve perfect momentum matching property in a broadband [8, 17]. The envelope line of the input of the Vivaldi slot can be written as follows: $y = C_1 e^{\alpha x} + C_2$, where $C_1 = \frac{y_1 - y_0}{e^{\alpha x_1} - e^{\alpha x_0}}$, $C_2 = \frac{y_0 e^{\alpha x_1} - y_1 e^{\alpha x_0}}{e^{\alpha x_1} - e^{\alpha x_0}}$ (($\times 0$, y_0) and ($\times 1$, y_1) are the coordinates of the starting and ending points of the slot line). Here, it is important to select the suitable value of α. If α is small, the length of the gradient transition region tends to be long. If α is large, the momentum matching property will be bad between the plasmonic waveguide and CPW. After simulation, it is found that good matching property is given when α varies from 1.8 to 2.2. So, we selected $\alpha = 2$ in the simulation and experiment. Part III is the interaction area consisted of plasmonic waveguide and CDR. The parameters of plasmonic waveguide and CDR are chosen as follows: R = 1200 μm, r = 600 μm, h_1 = 500 μm, h_2 = 450 μm, p = 380 μm, a = 0.5p, and N = 20 (the total number of grooves). The groove depths of plasmonic waveguide and CDR are determined to ensure that the cutoff frequency of plasmonic waveguide is greater than multipolar resonance frequency of CDR. The spacing g (shown in Fig. 1) is selected as 9.4 μm to achieve strong coupling between plasmonic waveguide and CDR. The surface metallic layer (gold) is 0.5-μm thick with the property similar to perfect conductor compared to visible region [18]. Quartz is used as the substrate with dielectric loss

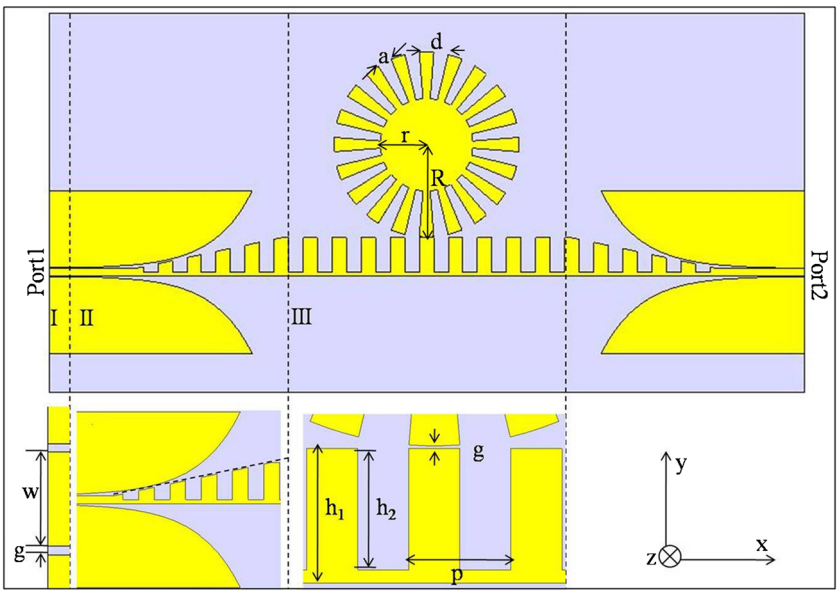

Fig. 1 Top view of the proposed plasmonic chip which is divided into three regions (I, II, and III). Part I: the CPW region. Part II: the convertor, which converts QTEM mode to plasmonic mode. Part III: plasmonic waveguide with CDR

tangent of tan(δ) = 0.0004 and thickness of 200 μm to reduce the loss.

The numerical simulation of the designed plasmonic chip was carried out by using commercial software, CST Microwave Studio. The boundary conditions of *x*, *y*, and *z* axes are set as open. The simulated transmission coefficient S_{21}(dB) of the proposed chips without (black curve) and with (red curve) CDR are shown in Fig. 2a. Transmission coefficient S_{21} is a scattering parameter of S-parameters, which means the response at port 2 due to a signal at port 1, where the first number in the subscript refers to the responding port, and the second number refers to the incident port. Thus, S_{21} is referred to as transmission coefficient, because it refers to what happens at output port when it is excited by a signal incident at input port. When the electromagnetic wave passes along the plasmonic waveguide and close to CDR, part of the transmitted field is coupled into the resonator and propagates around its surface. Only discrete frequencies can satisfy coherence condition and achieve destructive interference. Here, six main dips (marked as 1–6 in Fig. 2a) can be observed in the transmission spectrum (red curve) when CDR is placed and close to the waveguide. Such dips correspond to different spoof LSP resonances. To see this clearly, Fig. 2b–g illustrate the electric field (Ez) of dips corresponding to mode 1–6 in Fig. 2a on an *x*-*y* plane which is 0.1 mm above the metallic film. Multipolar resonances are sufficiently excited. From electric field

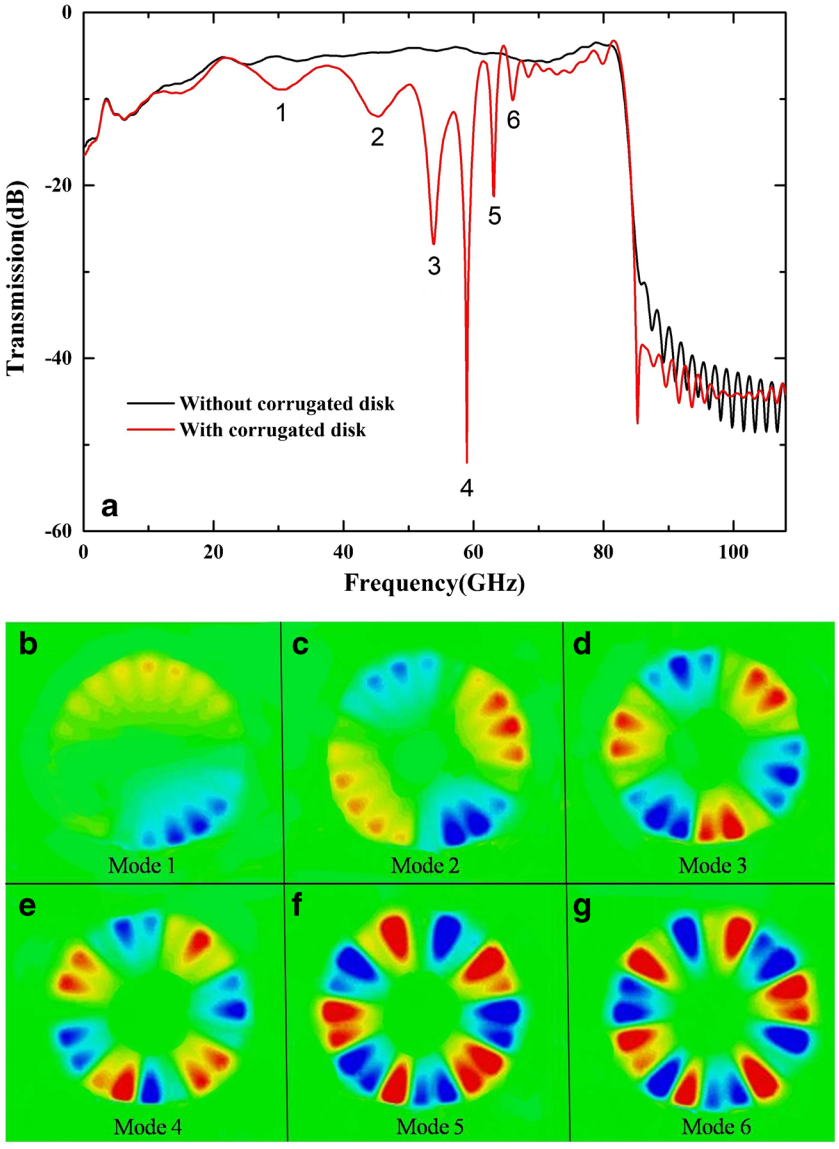

Fig. 2 **a** The transmission coefficient S21 of plasmonic waveguide chip without (with) CDR; **b**–**g** electric fields (E_z) on an x-y plane which is 0.1 mm above the metallic film

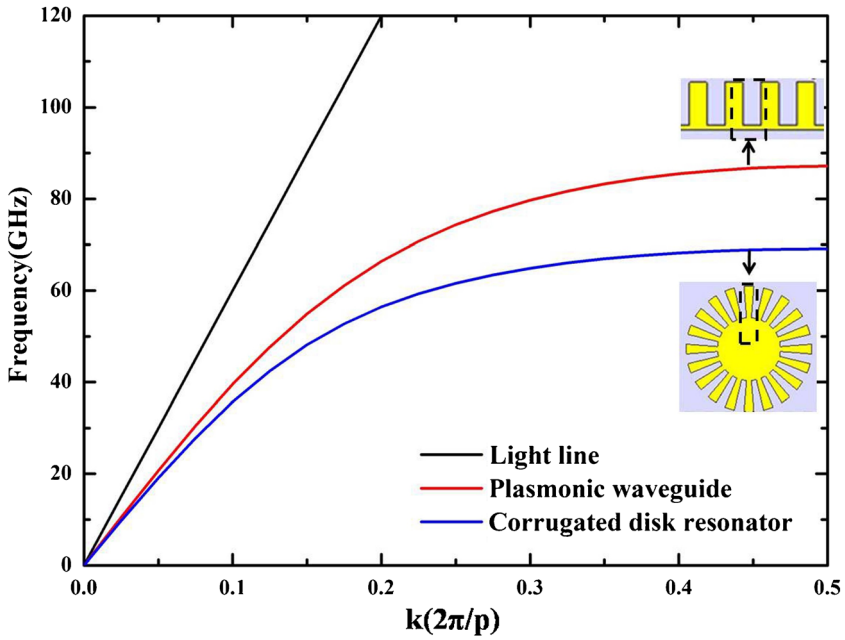

Fig. 3 The dispersion curves of plasmonic waveguide (*red curve*) and CDR (*blue curve*)

distributions shown in Fig. 2b–g, dips 1–6 are occurred in the transmission spectrum correspond to dipolar(1), quadrupolar(2), hexapolar(3), octupolar(4), decapolar(5), and dodecapolar(6) resonance modes. Specially, the resonance frequencies (Q factors) of hexapolar(3), octupolar(4), and decapolar(5) dips are 53.9 GHz(44.6), 59 GHz (283.4), and 63.2GHz (215.8), respectively. Here, the Q-value of multipoles mode with the unit dB in vertical ordinate is defined as follows: $Q = f_o/\Delta f$, where f_o is the center frequency and Δf is the full width at half maximum (under the unit dB) of the resonance dip in the transmission spectrum. This definition can help us easily observe the narrow line width in vertical ordinate with the unit dB [15].

The resonance frequencies shown in Fig. 2a can be derived by dispersion curve of CDR. The dispersion curves of plasmonic waveguide and CDR are shown in Fig. 3, where the black curve represents the light line and the red (blue) curve is the dispersion of plasmonic waveguide (CDR). The phase change due to CDR can be written as follows [19]:

$$\Delta\varphi = 2\pi \mathrm{R} \cdot \beta, \tag{1}$$

where β is the propagation constant. The coherence condition must be met for constructive (destructive) interference when the output wave is enhanced (closed); in other words, the circumference of the resonator must be an even (odd) number of wavelengths or frequencies of the resonant modes for constructive (destructive) interference, that is

$$\Delta\varphi = 2m\pi(\Delta\varphi = (2m+1)\pi). \tag{2}$$

In order to investigate the position of resonant dips, we focus on the destructive interference. Substituting Eq. (2) into Eq. (1), we get

$$(2m+1)\pi = \beta \cdot 2\pi \mathrm{R}. \tag{3}$$

If we define $k = \frac{\beta}{2\pi/p}$ is the normalized wavenumber ($p = \frac{2\pi R}{N}$ is the periodic constant of CDR), k can be rewritten as

$$k\left(\frac{2\pi}{p}\right) = \frac{\beta}{2\pi/p} = \frac{2m+1}{2R} \cdot \frac{p}{2\pi} = \frac{2m+1}{2N} \tag{4}$$

From Eq. (4), we can see k is linear to m. According to dispersion curve of CDR (blue line), the resonance frequencies of different modes are obtained. Table 1 lists the resonance frequencies (modes 3 ~ 5) derived by the dispersion

Table 1 Theoretical and numerical resonance frequencies of different modes

m	k (2π/p)	Frequency(GHz) from the dispersion curve	Frequency(GHz) from the S_{21} parameter
3	0.175	53.8	53.9
4	0.225	60.1	59.0
5	0.275	64.2	63.2

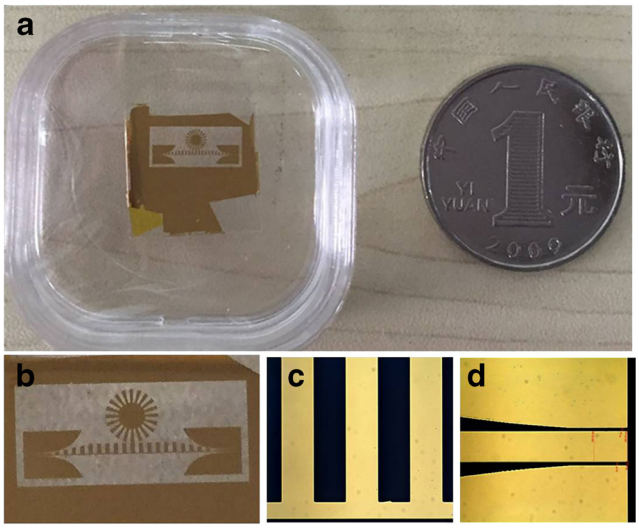

Fig. 4 **a**, **b** The photograph of the sample in a membrane box; **c**, **d** Optical microscope images of plasmonic waveguide and CPW

curve and Fig. 2a. The theoretical results fit well with the numerical ones.

Experiment

The sample of plasmonic waveguide chip is shown in Fig. 4. In the experiment, the total size of quartz substrate is 15 mm × 15 mm (Fig. 4b). The structure (CPW, plasmonic waveguide, and CDR) was fabricated by conventional lithography. First, the surface of quartz (substrate) was cleaned by acetone, methanol, and deionized water. Then, a layer of photoresist (AZ5214) was spin coated on one surface of quartz and prebaked on hotplate at 100 °C for 60 s to enhance the adhesion between photoresist and quartz substrate. A standard photolithography was then conducted before substrate was put into the developer solution. Finally, a gold layer (500 nm) was deposited with electron beam evaporation, after which a lift-off process helped form the final metallic pattern [20, 21]. Figure 4c–d are optical microscope images of plasmonic waveguide and CPW. The transmission coefficient S21 was measured by vector network analyzer (Agilent N5245 A, the frequency band is 50–75 GHz, which covers mode 3–5). The analyzer has two probes which are placed on both ends of the ports. Each of probes has three pins. In the experiment, the middle pin is contacted with the waveguide, and the other two pins are contacted with top and bottom gradient structures. Both probes are used as the signal source and the receiving end, respectively. The measured spectrum of S21 parameter is displayed on the computer.

The simulation and experiment results are shown in Fig. 5. The modes 3–5 are appeared clearly in the transmission spectra. The experimental (simulated) resonance frequencies are 53.7 GHz (53.9 GHz), 59.2 GHz (59.0GHz), and 63.3 GHz (63.2 GHz), respectively. And the experimental (simulated) transmission coefficient (dB) can reach −28.9 dB (−28.6 dB), −39.8 dB (−52.1 dB), and −18.1 dB (−21.3 dB), respectively. In experiment, the Q-value of octupolar mode was observed as high as 268.3, which is suitable for sensing application. Experimental result shows good agreement with simulation. The slight difference between simulation and experiment is caused by fabrication and measurement tolerances.

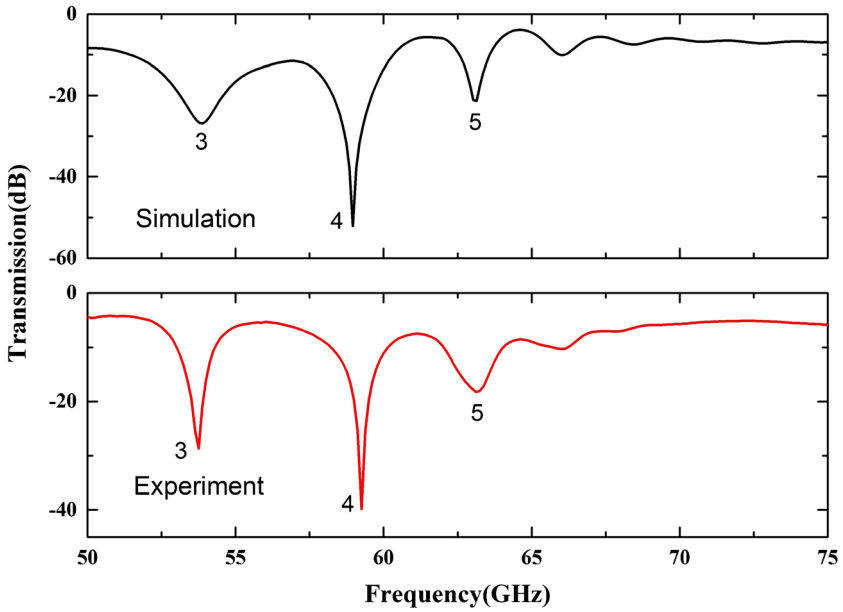

Fig. 5 Simulated and measured transmission coefficients S21 with CDR

Conclusion

In conclusion, we designed the millimeter plasmonic chip consisted of CPW and plasmonic waveguide with CDR. Six multipolar resonances can be found in the simulated transmission spectrum. These spoof LSP modes correspond to dipolar, quadrupolar, hexapolar, octupolar, decapolar, and dodecapolar resonance modes. The octupolar resonance dip shows Q factor as high as 268.3. The dispersion relation of CDR is used to verify the resonance frequencies of spoof LSP modes. Experimental results fit well with the simulated and theoretical ones. This multipolar plasmonic chip may have applications in sensing and circuits fields at millimeter and terahertz range.

Acknowledgments This work was partly supported by the National Program on Key Basic Research Project of China (973 Program, 2014CB339806), Basic Research Key Project (12JC1407100), Major National Development Project of Scientific Instrument and Equipment (2011YQ150021) (2012YQ14000504), National Natural Science Foundation of China (11174207) (61138001) (61205094) (61307126), Shanghai Rising-Star Program (14QA1403100), Program of Shanghai Subject Chief Scientist (14XD1403000), Hujiang Foundation of China (C14002), Zhejiang Key Discipline of Instrument Science and Technology (JL150505), and the New Century Excellent Talents Project from the Ministry of Education (NCET-12-1052).

References

1. Tonouchi M (2007) Cutting-edge terahertz technology. Nat Photonics 1:97–105
2. Reinhard B, Schmitt KM, Wollrab V, Neu J, Beigang R, Rahm M (2012) Metamaterial near-field sensor for deep-subwavelength thickness measurements and sensitive refractometry in the terahertz frequency range. Appl Phys Lett 100:221101
3. Singh R, Cao W, Al-Naib I, Cong L, Withayachumnankul W, Zhang W (2014) Ultrasensitive terahertz sensing with high-Q Fano resonances in metasurfaces. Appl Phys Lett 105:171101
4. Ng B, Wu J, Hanham SM, Fernández-Domínguez AI, Klein N, Liew YF, Breese MB, Hong M, Maier SA (2013) Spoof plasmon surfaces: a novel platform for THz sensing. Adv Opt Mater 1(8):543–548
5. Chen L, Gao CM, Xu JM, Zang XF, Cai B, Zhu YM (2013) Observation of electromagnetically induced transparency like transmission in terahertz asymmetric waveguide-cavities systems. Opt Lett 38(9):1379–1381
6. Chen L, Xu JM, Gao CM, Zang XF, Cai B, Zhu YM (2013) Manipulating terahertz electromagnetic induced transparency through parallel plate waveguide cavities. Appl Phys Lett 103: 251105
7. Mendis R, Astley V, Liu J, Mittleman DM (2009) Terahertz microfluidic sensor based on a parallel-plate waveguide resonant cavity. Appl Phys Lett 95(17):171113
8. Chen L, Cheng ZX, Xu JM, Zang XF, Cai B, Zhu YM (2014) Controllable multiband terahertz notch filter based on a parallel plate waveguide with a single deep groove. Opt Lett 39:4541–4544
9. Chen L, Zhu YM, Zang XF, Cai B, Li Z, Xie L, Zhuang SL (2013) Mode splitting transmission effect of surface wave excitation through a metal hole array. Light Sci Appl 2:e60
10. Driscoll T, Andreev GO, Basov DN, Palit S, Cho SY, Jokerst NM, Smith DR (2007) Tuned permeability in terahertz split-ring resonators for devices and sensors. Appl Phys Lett 91(6):062511
11. Withayachumnankul W, O'Hara JF, Cao W, Al-Naib I (2014) Limitation in thin-film sensing with transmission-mode terahertz time-domain spectroscopy. Opt Express 22(1):972–986
12. Ma H, Shen X, Cheng Q, Jiang W, Cui T (2014) Broadband and high-efficiency conversion from guided waves to spoof surface plasmon polaritons. Laser Photonics Rev 8(1):146–151
13. Zhang H, Liu S, Shen X (2015) Broadband amplification of spoof surface plasmon polaritons at microwave frequencies. Laser Photonics Rev 9:83–90
14. Pan BC, Liao Z, Zhao J, Cui TJ (2014) Controlling rejections of spoof surface plasmon polaritons using metamaterial particles. Opt Express 22:13942
15. Chen L, Wei YM, Zang XF, Zhu YM, Zhuang SL (2016) Excitation of dark multipolar plasmonic resonances at terahertz frequencies. Sci Rep 6:22027
16. Shen XP, Cui TJ (2013) Planar plasmonic metamaterial on a thin film with nearly zero thickness. Appl Phys Lett 102(21):211909
17. Chio T, Schaubert DH (2000) Parameter study and design of wide-band widescan dual-polarized tapered slot antenna arrays. IEEE Trans Antennas Propag 48(6):879–886
18. Shen XP, Cui TJ (2014) Ultrathin plasmonic metamaterial for spoof localized surface plasmons. Laser Photonics Rev 8(1):137–145
19. Chen L, Cao ZQ, Ou F, Li HG, Shen QS, Qiao HC (2007) Observation of large positive and negative lateral shifts of a reflected beam from symmetrical metal-cladding waveguides. Opt Lett 32(11):1432–1434
20. Wei YM, Chen CY, Chen L (2016) Study on etching process of silicon based periodic groove structure. Optical Instruments 38(3): 272–277
21. Shan Y, Xu BQ, Chen L (2015) Preparation and morphology influence of porous silicon by electrochemical etching conditions. Optical Instruments 37(1):9–13